Evaluation of Positive-Definite and Monotonic Limiters for Scalar Advection in the Advanced Research WRF

Hailong Wang[1, 3], William C. Skamarock[2], and Graham Feingold[3]

[1]CIRES, University of Colorado, Boulder, CO, USA
[2]National Center for Atmospheric Research, Boulder, CO, USA
[3]NOAA Earth System Research Laboratory, Boulder, CO, USA

1. Introduction

As a fundamental process in fluid dynamics, advection is of central importance in atmospheric transport of energy, water and chemical species. In atmospheric modeling, numerical diffusion and dispersion errors induced by the treatment of advection can dominate over related physical processes. Especially, sharp gradients and discontinuities in scalar quantities, such as cloud condensation nuclei (CCN) number concentration, cloud water mass and droplet number concentration, make the numerical treatment of advection more challenging. Without adequate treatment of this problem, simulations of cloud and precipitation processes could be ambiguous or misleading. Hence, when numerically modeling advection, the aim is to minimize diffusion and dispersion errors, provided the scheme's stability and efficiency are acceptable.

In the officially released version 3.0 of the Advanced Research Weather Research and Forecasting (ARW) model, the advection of scalars is performed using the third order Runge-Kutta (RK3) time-integration scheme (Skamarock et al. 2008). Spatial discretizations for momentum and scalar advection are accurate to 2nd through 6th order. The even-order schemes contain no implicit numerical diffusion, while the odd-order schemes are inherently diffusive with a diffusion term proportional to the Courant number. However, the even-order schemes tend to be more dispersive (e.g., Anderson and Fattahi 1974). The basic RK3 scheme is conservative, but it is neither positive definite (PD) nor monotonic. PD means that no non-physical negative mixing ratios are generated by the advection scheme, while monotonicity implies that the scheme does not generate new minima and maxima. For cloud-resolving modeling studies and many other applications it may be desirable to use monotonic advection schemes for scalar transport.

In this study, both PD and monotonic limiters (Skamarock 2006; Zalesak 1979), as described in the appendix, are applied to the basic RK3 scheme and are evaluated by examining the advection of passive tracers, CCN and cloud droplets in three-dimensional large-eddy simulations.

Corresponding author address: Hailong Wang, 325 Broadway, Boulder, CO 80305, USA.
Email: Hailong.Wang@noaa.gov

2. Numerical Experiments

Large-eddy simulations (LES) of marine stratocumulus clouds were performed using the ARW model (Skamarock et al. 2008) including the treatment of aerosol-cloud interactions. A double-moment warm-rain microphysical scheme initially developed by Feingold et al. (1998) has been modified and incorporated in ARW V3.0. This scheme uses lognormal basis functions to represent CCN, cloud droplet and drizzle drop spectra. Details of the microphysical scheme and initialization of model simulations are described by Wang and Feingold (2008).

Six numerical experiments (RK53, PD53, MO53, RK64, PD64 and MO64) with different advection schemes were conducted in a 10 x 10 km^2 domain with a uniform grid spacing of 100 m in the horizontal and ~30 m in the vertical. In the experiment names, “RK”, “PD” and “MO” indicate use of the basic RK3 advection with no limiter, with the PD limiter and with the monotonic limiter, respectively. The horizontal flux calculation is accurate to 5th (6th) order and the vertical to 3rd (4th) order, as denoted by “53” (“64”). TKE closure is used to calculate the sub-grid scale scalar diffusion. Periodic boundary conditions are assumed in both the x and y directions. The model depth is 1.5 km with a damping layer in the upper 250 m. Given the wind speed of about 10 m s^{-1} and the time step of 1 s, the Courant typical number is small, about 0.1.

Passive tracers were initially homogeneously distributed in four cubes with concentration of 1 and zero elsewhere in the model domain. Each cube is 2.5 x 2.5 x 0.9 km^3 in volume. Mass and number concentration of cloud droplets and rain drops are predicted using the double-moment microphysical scheme. The initial CCN number concentration was assumed to be 100 cm^{-3} for the entire model domain. Aside from transport, activation of cloud droplets is the only sink and evaporation of drops is the only source of CCN. No replenishing source is

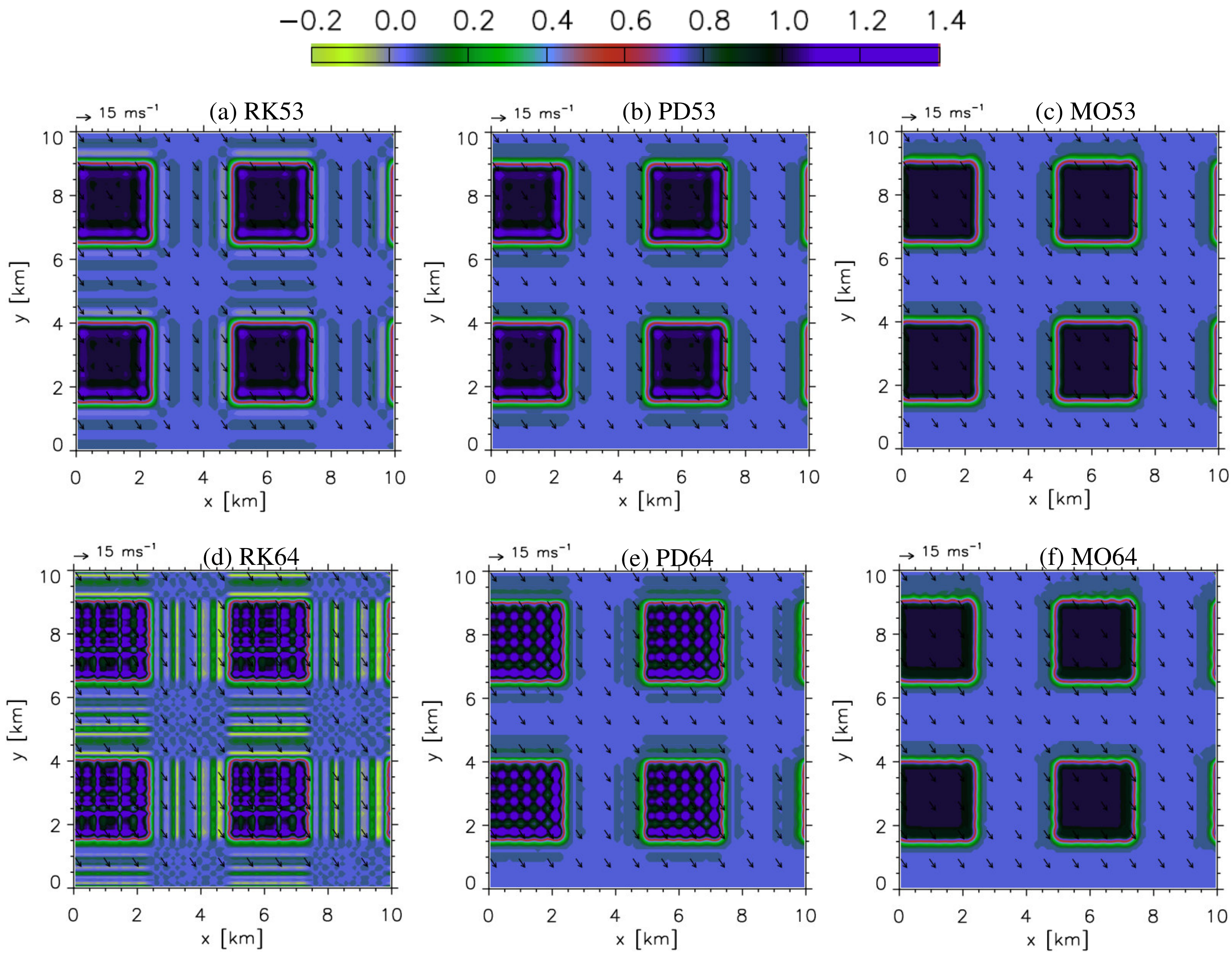

Figure 1: Horizontal cross section of tracer concentrations at about 750 m after 600 time steps (10 minutes) for experiments (a) RK53, (b) RK64, (c) PD53, (d) PD64, (e) MO53, and (f) MO64 with superimposed wind vectors.

used. Hence, only drop collection and precipitation can deplete CCN.

3. Results

Figure 1 shows the horizontal cross section of the tracer concentration field 10 minutes into the simulation. As expected, without any flux limiter the basic RK3 advection scheme produces significant spurious oscillations inside and outside of the tracer cubes. Negative tracer concentrations are produced near the sharp gradients. The PD limiter removes negative values but oscillations still exist. The local maxima inside the cubes are amplified by up to 30%. The monotonic limiter not only prevents negative tracer concentrations but also effectively avoids overshooting and preserves the sharp gradients. When the advection schemes with higher even-order accuracy are applied, numerical dispersion errors are larger than in corresponding lower odd-order ones. The ripple waves become stronger and shorter. Moreover, numerical diffusion errors are clearly seen inside the tracer cubes in the case with monotonic limiter. These test results indicate that the 5^{th} (3^{rd}) order horizontal (vertical) approximation for spatial derivatives performs better than the 6^{th} (4^{th}) order scheme.

A similar response of the CCN and cloud droplet number concentrations (CDNC) to the different advection schemes is observed. However, because these scalars are actively involved in physical processes, it is unwise to compare instantaneous fields in a point-by-point manner as given for the passive tracers in Figure 1. Figure 2 shows the frequency distribution of CCN concentration and CDNC at the end of the 4^{th} simulation hour. Although CCN in the boundary layer have been highly depleted by activation and collection processes, a significant number of grid volumes above the boundary layer have CCN concentrations greater than 100 cm^{-3} in both the RK53 and PD53 cases. Compared to the monotonic limiter, the PD limiter causes significant reductions in CDNC and CCN concentration in the boundary layer. Shifts in the frequency peaks are clearly seen. The median value of CCN concentration (CDNC) for RK53, PD53 and MO53 is 63.0 (19.3), 55.1 (10.1) and 65.7 (17.6), respectively. We expect that the PD limiter and the monotonic limiter could have substantially different impact on cloud microphysical and macrophysical properties due to both scalar advection and feedbacks through physical processes. For example, the lower CDNC in PD53 compared to MO53 could accelerate the formation of precipitation, which would result in further reductions in CCN and CDNC.

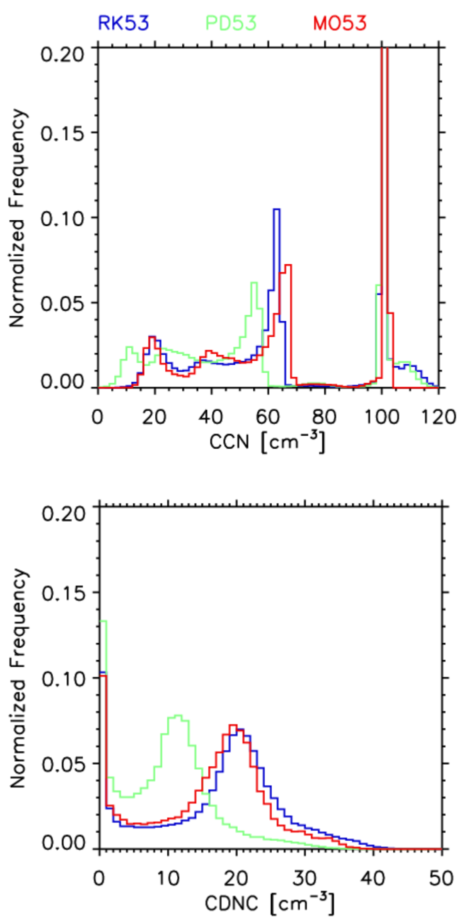

Figure 2: Histogram of CCN concentration and cloud droplet number concentration (CDNC) at the end of the 4th simulation hour for RK53, PD53 and MO53.

Figure 3 shows an example of how the PD limiter may lead us to misunderstanding of the cloud physical processes. Physically, higher concentrations of CCN right above cloud top derive from evaporation of detrained cloud droplets. With the monotonic limiter CCN concentrations are enhanced by up to 3%. However, the PD limiter highly exaggerates this physical effect. The CCN concentrations above clouds are enhanced by up to 20%. As a result, CDNC and CCN concentrations in and below cloud are reduced, as also shown in Figure 2.

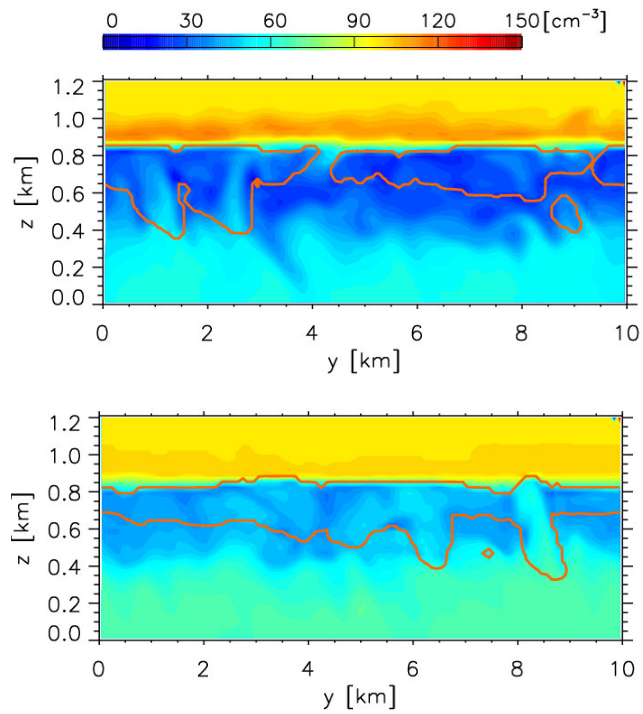

Figure 3: Vertical cross section of total particle (CCN + drop) number concentration (shaded colors) at the end of the 4th simulation hour for PD53 (top) and MO53 (bottom); Orange lines represent the 0.01 g kg^{-1} cloud water mixing ratio contour.

4. Summary

The basic third-order Runge-Kutta (RK3) time-integration scheme, together with positive definite and monotonic limiters based on flux renormalization, has been tested for scalar transport in fine-resolution ARW simulations. Without any flux limiter the RK3 scheme produces spurious oscillations in scalar concentrations. Clipping of non-physical negative values destroys the scalar conservation by retaining amplified local maxima. Appling the positive-definite flux limiter not only removes the negative values but also reduces the oscillations. However, amplification of local maxima is still as large as 30%. These numerical dispersive errors can cause problems directly and indirectly through feedbacks with physical processes. The monotonic limiter applied to the RK3 scheme, described in the appendix, effectively minimizes the dispersive errors at a cost of 8% more computational time, compared to 7% due to the PD limiter. No significant enhancement of numerical diffusion error is noticed, likely, because the Courant number was small.

Another set of simulations tested the impact of different order-of-approximation for spatial derivatives in advection schemes. Overall, simulation results show that the lower odd-order accuracy of the advection schemes cause less numerical dispersion error than even-order ones.

In summary, the sensitivity tests in this study suggest that the RK3 scheme with a monotonic flux limiter using 5th (3rd) order horizontal (vertical) accuracy is recommended for scalar advection in ARW model, at least for fine-resolution cloud modeling such as that presented here.

5. Appendix

The PD limiter has been described in Skamarock and Weisman (2008). Here we focus on describing the formulation of monotonic RK3 scalar transport in the ARW model. The final step of the discrete integration of scalar conservation equation,

$$\frac{\partial \mu\phi}{\partial t}+\frac{\partial \mu u\phi}{\partial x}+\frac{\partial \mu v\phi}{\partial y}+\frac{\partial \mu\dot{\eta}\phi}{\partial \eta}=\mu S_\phi\,, \quad (1)$$

by RK3 can be written as

$$(\mu\phi)^{t+\Delta t}=(\mu\phi)^{t}-\Delta t\left(\sum_i \delta_{x_i}F_{x_i}^{**}-\mu S_\phi^t\right), \quad (2)$$

where ϕ is the scalar mixing ratio, μ the column mass, F the flux of ϕ and S the source/sink term (i.e., the physical tendencies and explicit mixing). $\delta_{x_i}F_{x_i}^{**}$ denotes the centered flux divergence operator in the ith coordinate direction at the previous RK3 step, $t+\Delta t/2$. When introducing the monotonic limiter (Skamarock 2006), Eq. (2) is replaced by

$$(\mu\phi)^{***}=(\mu\phi)^{t}+\Delta t\,\mu S_\phi^t\,, \quad (3a)$$

$$(\mu\phi)^{t+\Delta t}=(\mu\phi)^{***}-\Delta t\sum_i \delta_{x_i}\left[F_{x_i}^{1***}+R\left(F_{x_i}^{cor**}\right)\right], \quad (3b)$$

Here $F_{x_i}^{1***}$ is the first-order upwind flux computed using Eq. (3a), and the high-order flux correction $F_{x_i}^{cor**}$ is calculated as

$$F_{x_i}^{cor**}=F_{x_i}^{**}-F_{x_i}^{1***}\,. \quad (4)$$

The renormalized high-order flux correction $R(F_{x_i}^{cor**})$ is obtained through the following procedure. First, the scalar mass is updated using Eq. (3a) and the first-order upwind fluxes as

$$(\tilde{\mu\phi})=(\mu\phi)^{***}-\Delta t\sum_i \delta_{x_i}F_{x_i}^{1***}\,. \quad (5)$$

Next, minimum and maximum updated mass are estimated using

$$(\tilde{\mu\phi})_{\min}^{t+\Delta t}=(\tilde{\mu\phi})-\Delta t\sum_i \delta_{x_i}\left(F_{x_i}^{cor**}\right)^{+}, \quad (6a)$$

$$(\tilde{\mu\phi})_{\max}^{t+\Delta t}=(\tilde{\mu\phi})-\Delta t\sum_i \delta_{x_i}\left(F_{x_i}^{cor**}\right)^{-}, \quad (6b)$$

where $(\ )^{+}$ and $(\ )^{-}$ denotes outgoing and incoming flux, respectively. Finally, renormalization of the outgoing and incoming high-order flux correction is done by

$$R\left(F_{x_i}^{cor**}\right)^{+}=\left(F_{x_i}^{cor**}\right)^{+}\cdot\min\left(1.0,\frac{(\tilde{\mu\phi})-(\mu\phi_{\min})}{(\tilde{\mu\phi})-(\tilde{\mu\phi})_{\min}^{t+\Delta t}}\right), \quad (7a)$$

and

$$R\left(F_{x_i}^{cor**}\right)^{-}=\left(F_{x_i}^{cor**}\right)^{-}\cdot\min\left(1.0,\frac{(\tilde{\mu\phi})-(\mu\phi_{\max})}{(\tilde{\mu\phi})-(\tilde{\mu\phi})_{\max}^{t+\Delta t}}\right), \quad (7b)$$

where $\phi_{\max}$ and $\phi_{\min}$ are maximum and minimum scalar mixing ratio in central and upwind cells at time t.

After applying Eqs. (7a) and (7b) to Eq. (3b), formulation of monotonic RK3 advection scheme is completed.

6. Acknowledgements

We acknowledge support from NOAA's Climate Goal. Hailong Wang is supported by the Cooperative Institute for Research in Environmental Sciences (CIRES) Post-doctoral Fellowship. We thank Hongli Jiang, Adrian Hill, and Mary Barth for thoughtful discussions.

7. References

Anderson, D., and B. Fattahi, 1974: A comparison of numerical solutions of the advective equations. *J. Atmos. Sci.*, **31**, 1500-1506.

Feingold, G., R. L. Walko, B. Stevens, and W. R. Cotton, 1998: Simulations of marine stratocumulus using a new microphysical parameterization scheme. *Atmos. Res.,* **47–48,** 505–528.

Skamarock, W. C., 2006: Positive-definite and monotonic limiters for unrestricted-time-step transport schemes. *Mon. Wea. Rev.*, **134**, 2241–2250.

Skamarock W. C., J. B. Klemp, J. Dudhia, D. O. Gill, D. M. Barker, M. Duda, H. Huang, W. Wang, and J. G. Powers, 2008: A description of the advanced research WRF version 3. NCAR Tech. Note.

Skamarock, W. C., and M. L. Weisman, 2008: The impact of positive-definite moisture transport on NWP precipitation forecasts. *Mon. Wea. Rev.*, submitted.

Wang, H., and G. Feingold, 2008: Modeling aerosol effects on the formation of pockets of open cells in marine stratocumulus using WRF model. The 9th Annual WRF Users' Workshop. Boulder, CO, USA.

Zalesak, S. T., 1979: Fully multidimensional flux-corrected transport algorithms for fluids. *J. Comput. Phys.*, **31**, 335-362.